Role of inter-particle friction in granular materials under three dimensional conditions — PARTICLES 2019

Shuhan. Yang[1], Wei. Zhou[1], Jiaying. Liu[1], Tianqi. Qi [1], Gang. Ma[1]

[1] State Key Laboratory of Water Resources and Hydropower Engineering Science
Wuhan University
8 Donghu South Road, 430072 Wuhan, China
E-mail: yang-sh@whu.edu.cn(Shuhan Yang); zw_mxx@whu.edu.cn (Wei Zhou)

Key words: DEM, Inter-particle Friction, True Triaxial Tests, Strong and Weak Contact System, Coordination Number, Anisotropy.

Abstract. The inter-particle friction is known to be an important contributor to the strength and deformation characteristics in granular materials. The mechanism of inter-particle friction to the macroscopic responses can be explained by microscopic investigations. Based on the discrete element method (DEM), a series of true triaxial tests for the cubic granular assembly are carried out and the effects of inter-particle friction coefficient (μ) on the evolutions of macro- and micromechanical parameters of granular materials are studied. The macroscopic stress, the distribution of coordination numbers and contact force with regard to strong and weak contact networks are concerned, as well as the corresponding fabric tensor and anisotropies. Findings indicate that increasing inter-particle friction sharpens the peak value of deviatoric stress and enhances the degree of dilatancy of the granular assembly at the macroscopic level. From the microscopic perspective, the distribution of the coordination number of the weak contact system varies dramatically, while the number of particles with smaller coordination number in the strong contact system changes little with different μ. Besides, the difference between strong and weak contact networks is enlarged, and anisotropy indicators are significantly enhanced, which strengthen the bearing ability of anisotropic stresses in granular materials.

1 INTRODUCTION

Granular materials are closely linked to our daily life. Many important infrastructures concerning the quality and safety of our everyday life, such as rockfill dams, dikes and foundations, are built with geotechnical friction-dissipative granular materials. The performance of granular materials under external loads directly affects the design, construction and operation of these structures [1]. Under shear, granular materials exhibit extremely complex mechanical behaviors at the macroscopic level while the typical multi-scale features contribute a lot to the overall complexity [2]. The granular materials are composed of discrete particles whose macroscopic responses are vitally interrelated to their interaction. Inter-particle friction as one of the key factors affecting the interplay between particles, may significantly contribute to the macro- and micro-responses of granular materials.

DEM (Discrete Element Method) has demonstrated its ability in reproducing the

macroscopic responses and exploring the microscopic mechanism of granular materials [3]. Based on DEM simulations of granular assemblies, contact orientation [4, 5], force transmission [6, 7], contact networks [14] are regarded as the important characterization of the microstructure. Besides, the fabric tensor [9, 10, 11, 12] has been defined to measure the intensity and orientation of the contact texture anisotropy.

The interplay between particles is the intrinsic factor that causes the macroscopic responses of granular materials. To figure out the effects of inter-particle friction on granular materials, Rothenburg et al. [13] observed the relationship between void ratio and coordination number along different inter-particle friction by biaxial tests. Huang et al. [14] evaluated the sensitivity of critical state behaviors to inter-particle friction. Maya et al. [15] identified that increasing inter-particle friction promotes the formation of straighter chains and a greater degree of branching in the force chain network by two-dimensional simulations. Antoy et al. [16] investigated how particle-scale friction affect the mechanism of mobilization of macroscopic shear strength by conventional triaxial tests. However, true triaxial tests are rarely used in these simulations, which can reflect the real situation in nature or engineering.

The main purpose of this paper is to investigate the effects of inter-particle friction on the characteristic behaviors of granular materials under true triaxial tests. The stress–strain relationships and peak state of deviatoric stress are presented. From the view of strong-weak contact network, the micro-responses are explored, including the coordination number, the contact force, the fabric tensors and the anisotropies. The contribution of micro-investigations to macro-mechanical properties is further discussed.

2 DEM SIMULATIONS OF TRUE TRIAXIAL TESTS

2.1 Stress-strain invariants

The stress invariants describing true triaxial stress state are generalized shear stress q, average hydrostatic pressure p and Lode angle θ_σ:

$$p = \frac{\sigma_1 + \sigma_2 + \sigma_3}{3} \tag{1}$$

$$q = \frac{1}{\sqrt{2}}\sqrt{(\sigma_1 - \sigma_2)^2 + (\sigma_2 - \sigma_3)^2 + (\sigma_3 - \sigma_1)^2} \tag{2}$$

$$\tan\theta_\sigma = \frac{\sqrt{3}b}{2-b}, \quad b = \frac{\sigma_2 - \sigma_3}{\sigma_1 - \sigma_3} \tag{3}$$

The intermediate principal stress ratio b responses the relative magnitude of the intermediate principal stress σ_2 between the minor principal stress σ_3 and the major principal stress σ_1. The range of b is $0 \le b \le 1$. The Lode angle θ_σ defines the angle between the major principal stress and the deviatoric part of stress in the principal stress space. The true triaxial test with b = 0.0 represents the triaxial compression test ($\sigma_2 = \sigma_3$, θ_σ=0) and b = 1.0 indicates the traxial extension test ($\sigma_1 = \sigma_2$, $\theta_\sigma = \pi/3$).

2.2 Sample preparation and loading paths

The numerical sample is composed of 31 253 non-contacting spherical particles with Gaussian distribution in a 400mm×400mm×400mm cube. The minimum and maximum

particle sizes are 2 and 8.5 mm, respectively. Fig.1 shows the particle size distribution (PSD). In order to generate isotropic samples in the initial fabrics, we use the displacement control to compress the samples with a constant-speed in all directions until the target size. After that, isotropic consolidation is carried out and three-dimensional isobaric stress is applied to the specimen until the desired confining pressure 0.5 MPa is reached. Finally, the initial void ratio of the specimen is 0.582. The Hertz–Mindlin contact model is adopted. The inter-particle friction coefficient μ during loading process is set as 0.05, 0.1, 0.2, 0.3, 0.4 and 0.5, respectively, and other numerical parameters are shown in Table 1.

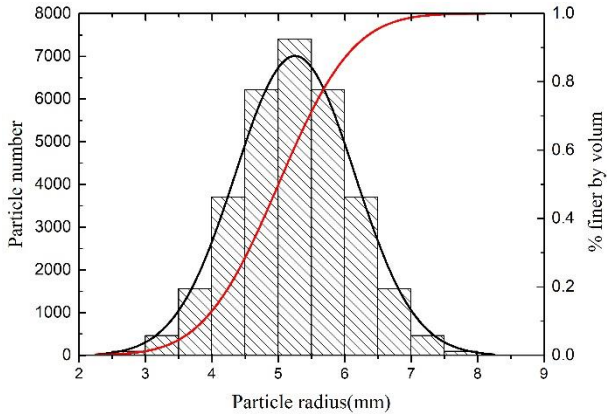

Fig.1 Radius distribution

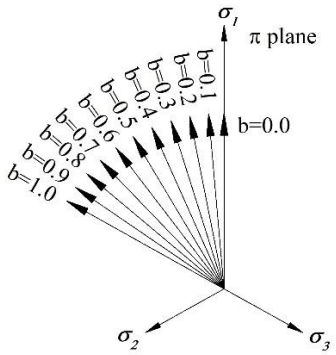

Fig.2 Stress path under true triaxial tests

Table1: Microscopic parameters of numerical simulation

Parameters	Value
Density ρ/(kg/m^3)	2600
Particle radius *d*/mm	2-8.5
Young's modulus *E*/GPa	65.0
Poisson's ratio *v*	0.4
coefficient of restitution *e*	0.95
sliding friction coefficient μ	0.05,0.1,0.2,0.3,0.4,0.5

In this paper, a series of true triaxial tests are under the constant-*p* and constant-*b* loading condition, and the stress paths are shown in Fig.2. In order to eliminate the boundary influence and avoid the occurrence of strain localization, these tests are carried out with periodic boundary. The stress in each direction of the specimen is controlled by the migration rate of periodic boundary. The intermediate principal stress σ_2 and minor principal stress σ_3 can be estimated from Eq. (4) and Eq. (5) respectively:

$$\sigma_2 = b\sigma_1 + (1-b)\frac{3p-\sigma_1(1+b)}{(2-b)} \quad (4)$$

$$\sigma_3 = \frac{3p-\sigma_1(1+b)}{(2-b)} \quad (5)$$

3 MACRO-SCALE RESPONSES

For various inter-particle friction, the evolution curves of generalized shear stress q and volumetric strain ε_v along deviatoric strain ε_d are shown in Fig. 3 (the positive volumetric strain represents contraction, negative value represents dilation). Increase in inter-particle friction μ steadily raises the shear strength of a granular assembly (the peak deviatoric stress) while the peak value occurs at a similar strain level (about 6%) irrespective of various μ. The deviatoric stress changes to a downward trend after reaching the peak value, which means strain softening. The larger inter-particle friction can enhance the strain softening behavior. In addition, diverse μ values lead to different volume responses of a granular assembly. Specifically, after a small compression deformation, the specimens are all in the dilatation condition. The particle assembly with large inter-particle friction starts the dilatation state earlier and shows a more evident dilatation degree at later stage of loading.

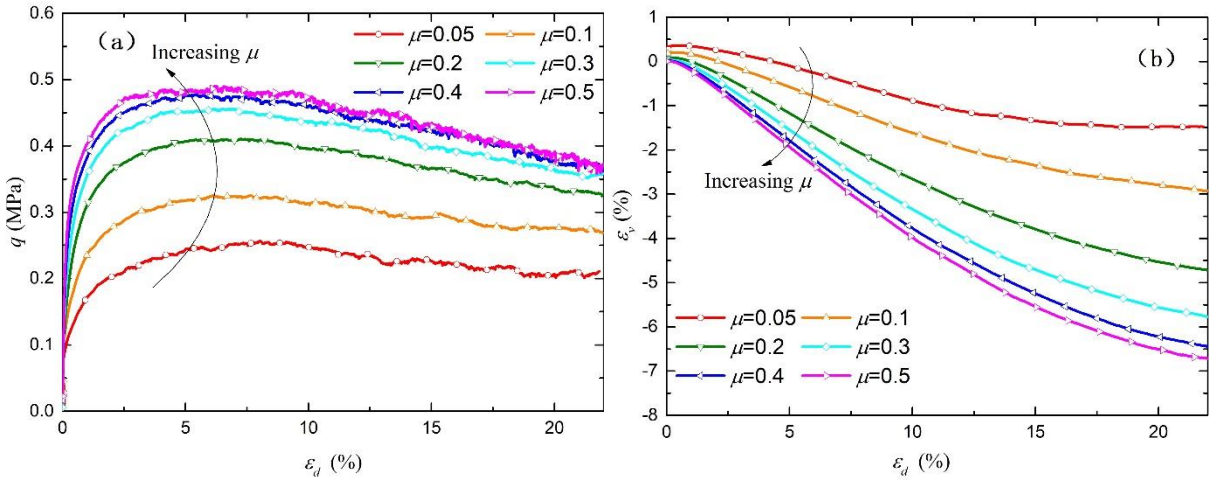

Fig.3 Macroscopic response of granular assemblies with different inter-particle friction: evolution of deviatoric stress (a) and volumetric strain (b) versus deviatoric strain ε_d

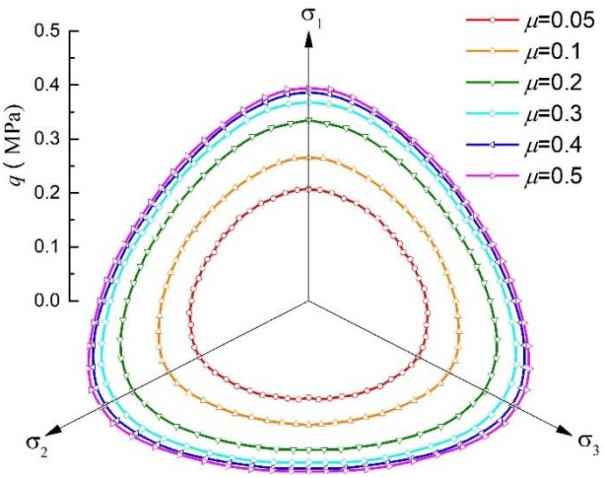

Fig.4 Peak state of deviatoric stress along different friction coefficients

Corresponding to different inter-particle friction, the three-dimensional stress surfcae in π plane is plotted in Fig. 4. For each given μ, the curve presents similar shape like triangular cone but differs from one another in size. The stress evolution in π plane reflects the peak deviatoric stress of the granular assmebly at different b and μ values. It can be seen that, the peak deviatoric stress decreases with the increase of b but improves with the increase of μ. Moreover, the sensitivity of the specimen to inter-particle friction debases along with μ, for the smaller increaseing extent of deviator stress. The stress characteristics shown in Fig. 4 conform to the general rule of true triaxial test and are also consistent with the conclusions of other numerical tests [16, 17, 18].

4 COORDINATION NUMBER

The geometric stability of a granular assembly under mechanical loading is generally studied in the matter of its apparent coordination number Z (i.e., average number contacts of per particle) at a given stage of loading. As a mesoscopic scalar index of granular materials, average coordination number Z_t is given by $2N_c/N_p$ where N_c and N_p are the total number of contacts and particles in the specimen respectively. It can also reflect the overall volume change of a granular assembly. In generally, higher average coordination number is corresponding to smaller porosity, closer interaction between particles, and more stable/isotropic internal structure. On the contrary, the degree of anisotropy increases.

Radjai et al. [5] divided the whole contact network into two complementary sub-contact nectworks, a strong contact subnetwork and a weak contact network that carry normal contact forces larger and less than the average. The two contact networks have different mechanisms for the geometric stability of granular materials. In presenting the results, we have hereby separated the contributions of the weak contact network from the strong contact network, along with the total value. The strong contact network is denoted by Γ_{strong}, the part from the weak contact network by Γ_{weak}, and the entire contact network by Γ_{total}. Fig. 5 shows difference performance among the three contact networks in terms of the relationship between the average coordination number and the inter-particle friction in the triaxial compression condition. Under the given loading path, each contact network presents a law that Z_t decreases with the increase of μ, which confirms the macroscopic phenomenon that the dilatation degree of the specimen is more obvious with large μ. Besides, average coordination number in Γ_{weak} is larger than that of Γ_{strong}, reflecting stronger internal stability and higher isotropy of Γ_{weak}. Considering the relationship between the average coordination number and the volume deformation of granular materials, it indirectly shows that the weak contact network contributes greater to the deformation of a granular assembly.

In a granular media, the coordination number Z_t indicates an average over particles within contact networks while the number of contacts neighbors n varies from particle to particle. Bratberg et al. [19] recognized that the connectivity of a granular assembly should be given by the fraction P_n, defined by particles having n contact neighbors. From the study of Liu et al. [20], particles with fewer coordination numbers are in lower degree of restraint condition, corresponding to higher anisotropy. Conversely, particles are more stable and show isotropy feature.

From the distribution of coordination number at stress peak state in Fig. 6, the coordination number Z in accordance with the abscissa denotes P_n, and the corresponding ordinate refers to

the number of n adjacent particles in contact with a single particle. In the total contact network (Fig.6a), the maximum particle content changes from P_5 to P_4, meanwhile, all distribution curves seem to move left entirely with the increase of μ value. Evidently, some particles with $n\geq5$ contacts lose neighbor contacts, causing the number of particles with $n\leq4$ contacts increase. The distribution of coordination number within weak contact network (Fig.6b) is similar to that of the total contact network, while the maximum particle content moves from P_4 to P_3. From that, the anisotropy feature of Γ_{weak} is stronger than that of Γ_{total} and both of them diminish owing to the increase of μ.

It is interesting to take a quantitative look at the strong contact network (Fig.6c) whose distribution of coordination number is quite different from that of the total contact network. Thanks to the increase of μ value, the number of particles ($P_n\geq P_3$) decreases. However, μ value appears to have little effect on the number of particles whose coordination number is 1 and 2, whereas P_1 and P_2 constitute the end and main body of the force chain in the contact network. It shows that the number of particles forming the force chain accounts for 1/3 of the total number and does not fluctuate with the change of μ value, as if satisfying the most advantageous condition of particulate distribution. This demonstrates that the shear resistance of granular assembly can be mobilized by selecting relatively few benificial orientated contacts to transmit the greater than average contact force.

Compared with strong, weak and total contact network (Fig.6d), the three curves can be roughly considered as the left translation of the total contact network curve. For the total contact network, the weak contact network makes more contribution to the coordination number distribution than the strong contact network. The influence of inter-particle friction on coordination number distribution of Γ_{weak} is greater than that of Γ_{strong}. The weak contact network tends to be isotropic, balancing hydrostatic pressure of the granular media, dominating overall volume deformation; while the strong contact network has obvious anisotropic feature, and bear most of the deviatoric stress of the granular assembly (shown in next chapter).

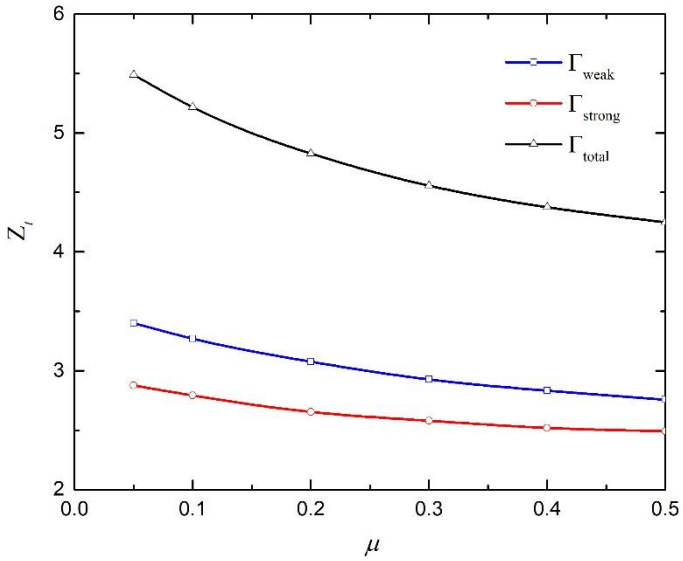

Fig.5 The relationship between the average coordination number and the inter-particle friction

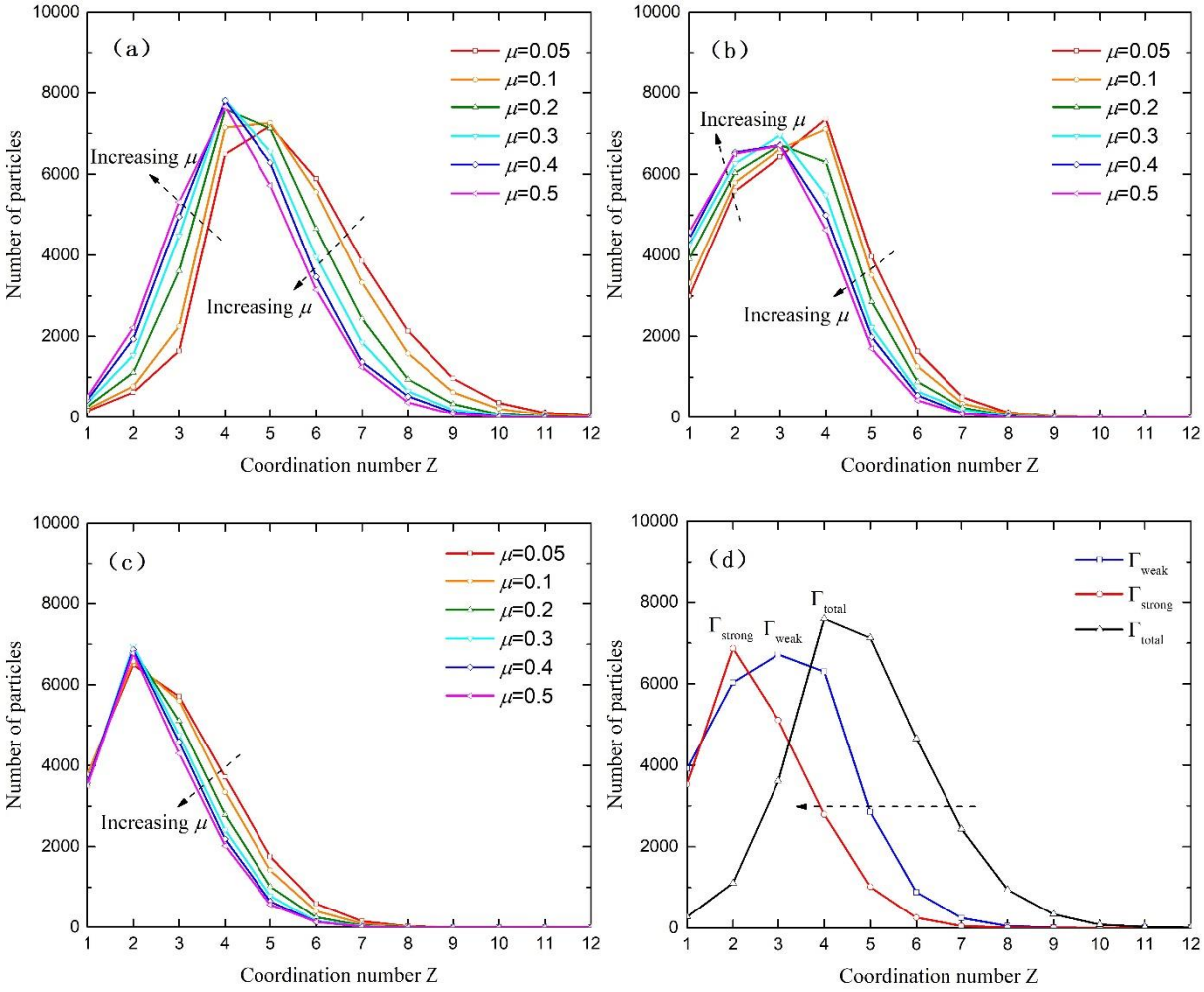

Fig.6 The distribution of coordination number at stress peak state: Number distribution of coordination number Z in the total contact network (a) the weak contact network (b) the strong contact network (c) and the comparison (d) while μ=0.2

5 FABRIC TENSOR AND ANISTROPY

5.1 Contact force

Radjai et al. [6] pointed out that the strong and weak contact network in a granular media have different mechanical mechanisms. Strong contacts have a decisive influence on the contribution of macro-mechanics. Fig. 7 shows the evolution of the average normal contact force and tangential contact force in the strong, weak and total contact network during true triaxial loading. The average normal contact force is much larger than the tangential contact force, indicating it's leading position. There is great disparity between the average normal contact force of strong and weak contact network, and the numerical relationship between them is about 4 times. For the total contact network, the evolution contribution of the average normal contact force is dominated by the strong contact network. With the increase of μ value, the normal contact force and tangential contact force in each contact network increase

obviously, while the average coordination number of them decreases. This reasonably explains the increase in the mechanic anisotropy feature of the granular assmebly (see Fig. 8), and highlights the supporting effect of the strong contact network on balancing external load.

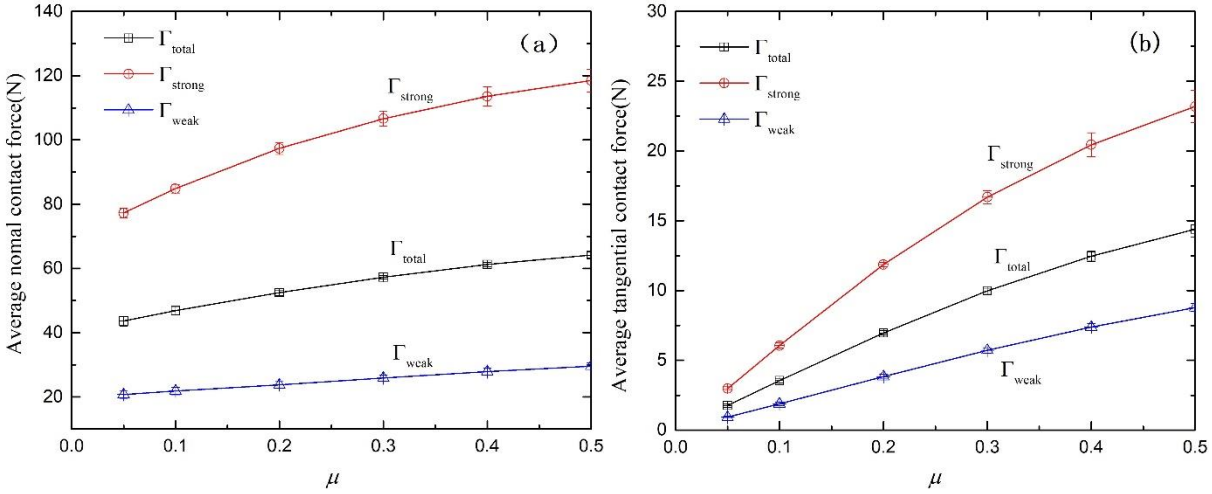

Fig.7 The relationship between contact force and inter-particle friction (a) Normal contact force (b) Tangential contact force

5.2 Definition of Contact Fabric Tensor

Based on the work of Yimsiri et al. [21] in quantitatively analyzing the anisotropy of a particle assembly, two classes of anisotropy with different mechanisms are differentiated: geometric anisotropy and mechanical anisotropy. The geometrical anisotropy is defined by the local orientation of contact plane which can be expressed by the distribution of contact normals and branch vectors. The mechanical anisotropy, however, is mainly created by the external forces and can be splited into normal force anisotropy (caused by normal contact forces) and tangential force anisotropy (induced by tangential contact forces). This paper adopts the following expression of fabric tensor proposed by Satake [22] and Oda [23]:

$$\Phi_{ij} = \int_{\Theta} E(\Theta) n_i n_j d\Theta \tag{6}$$

where ***n*** is the unit vector along the normal direction of the contact surface. Θ characterizes the orientation of ***n*** relative to the global coordination system. *E(Θ)* is the distribution probability density function, which can be expressed in terms of the second-order Fourier expansion:

$$E(\Theta) = \frac{1}{4\pi}(1 + \mathrm{a}_{ij}^{c} n_i n_j) \tag{7}$$

where the second-order anisotropy tensor a_{ij}^{c} is deviatoric and symmetric, which characterizes the geometrical anisotropy induced by normal contact.

$$\mathrm{a}_{ij}^{c} = 15/2\Phi_{ij}^{'} \tag{8}$$

where $\Phi_{ij}^{'}$ is the deviatoric part of the fabric tensor Φ_{ij}.

Only when the particle system is composed of non-spherical particles, the branch vector contributes greater to geometric anisotropy. The distribution of branch vectors can be expressed in the way similar to formula (7) and formula (8):

$$d_{ij} = \frac{1}{4\pi}\int_{\Theta} \overline{d}(\Theta) n_i n_j d\Theta \tag{9a}$$

$$\overline{d}(\Theta) = \overline{d}^{0}(1 + \mathrm{a}_{ij}^{l} n_i n_j) \tag{9b}$$

where a_{ij}^{l}=15/2（$d_{ij}^{'}/\overline{d}^{0}$）is the contribution value of branch vectors to the geometric anisotropic tensor. $\overline{d}^{0}$=d_{ii} is the average length of branch vectors in the domain Θ and $d_{ij}^{'}$ is the deviatoric part of d_{ij} .

The distribution function of normal contact force and tangential contact force are expressed respectively as (10b) and (11b). Correspondingly, the normal contact force tensor and the tangential contact force tensor are defined by equation (10a) and (11a).

$$\chi_{ij}^{n} = \frac{1}{4\pi}\int_{\Theta} \overline{f}^{n}(\Theta) n_i n_j d\Theta \tag{10a}$$

$$\overline{f}^{n}(\Theta) = \overline{f}^{0}(1 + \mathrm{a}_{ij}^{n} n_i n_j) \tag{10b}$$

and

$$\chi_{ij}^{t} = \frac{1}{4\pi}\int_{\Theta} \overline{f}^{t}(\Theta) t_i n_j d\Theta \tag{11a}$$

$$\overline{f}^{t}{}_{i}(\Theta) = \overline{f}^{0}\left[a_{ik}^{t} n_k - (a_{kl}^{t} n_k n_l) n_i\right] \tag{11b}$$

wherein $a_{ij}^{n} = \frac{15}{2}\frac{\chi_{ij}^{'n}}{\overline{f}^{0}}$, $a_{ij}^{t} = \frac{15}{2}\frac{\chi_{ij}^{'t}}{\overline{f}^{0}}$

$\overline{f}^{0} = \chi_{ii}^{n}$ is the average normal force in the domain Θ. The second-order anisotropy tensors $a_{ij}^{c}, a_{ij}^{l}, a_{ij}^{n}, a_{ij}^{t}$ are deviatoric and symmetric, then, the degree of anisotropy can be quantified by using the second invariants of the three anisotropy tensors defined above:

$$a_{*} = \sqrt{\frac{3}{2} a_{ij}^{*} a_{ij}^{*}} \tag{12}$$

where the sub/super-script * stands for contact normal, *c*, branch vector, *l*, normal contact force, *n*, and tangential contact force, *t*, respectively.

5.3 Characteristics and Evolution of Anisotropy

The characteristics of anisotropy and its evolution during the loading process are depicted in Fig.8. Owing to the use of spherical particles with a relatively narrow size distribution, the branch vector is almost in the same direction as contact normal vector and contributes so little to the total strength that can be ignored. The anisotropic coefficient of the initial specimen increases rapidly with the increase of the deviation strain, and the increase rate becomes more sharply with larger inter-particle friction. It can be seen evidently that the peak value of the normal contact force anisotropy a^{n} (about 3% of the deviatoric strain) comes earlier than that of the contact normal anisotropy a^{c} (about 6% of the deviatoric strain), and the peak value is higher than the latter. With the increase of μ value, the difference is more obvious. Interestingly, the contact tangential force anisotropy a^{t} reaches its peak within 1% of the

deviatoric strain, then decreases slightly and remains stable. Compared with the two mechanical anisotropy coefficients, the contribution of the tangential contact force anisotropy a^t to the anisotropy of the whole system is significantly less than that of the normal contact force anisotropy a^n.

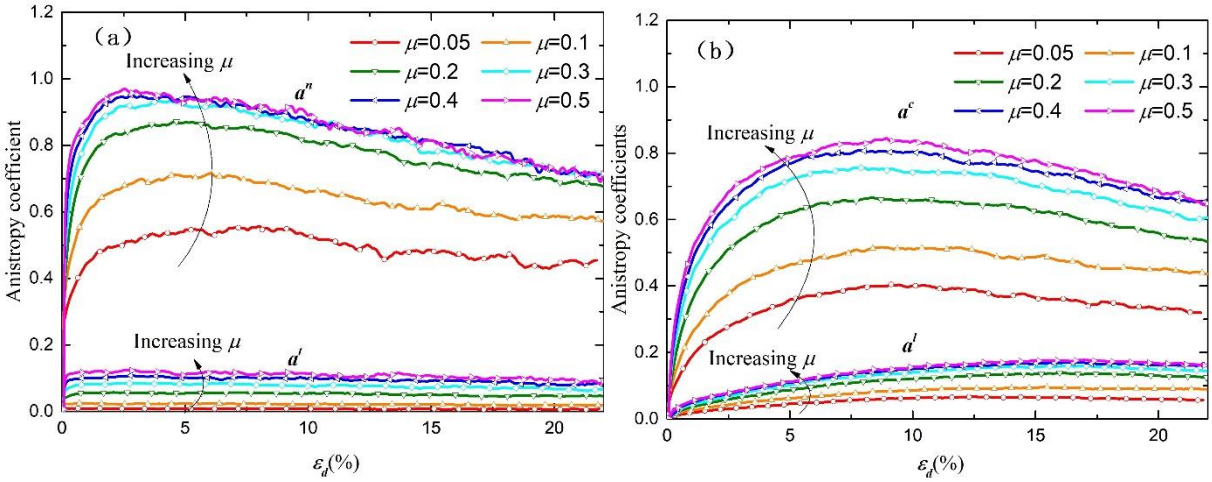

Fig.8 Anisotropy coefficient evolution curve (a) geometric anisotropy (b) mechanical anisotropy

The initial state, loading path and final size of the granular assembly are all the same under the true triaxial tests. Because of different inter-particle friction, great changes happen in the contact structure of the granular assembly. The average coordination number Z_t decreases, while the contact force enlarges, and the degree of anisotropy increases. The stark contrast between strong and weak contact forces is more striking, which effectively stimulates the anistropy of strong contact network and mobilizes shear strength to banlance external loads. Meanwhile, larger inter-particle friction makes the tangential contact point more difficult to destroy, which is conducive to the formation of the strong normal support to ensure that the granular assembly has a close contact state and maintain stability.

6 CONCLUSIONS

This paper has made a contribution to advance fundamental understanding of granular material response by considering the effects of inter-particle friction on the material response. Using DEM simulations of true triaxial tests, we have presented alternative ways to link the evolution of micro-mechanical parameters to the macro-scale behaviour of granular materials. The primary findings drawn from this qualitative study are the followings:

- In the constant-p and constant-b true triaxial tests, the macro stress-strain relationship of the granular assembly conforms to the existing physical and numerical results. With the increase of inter-particle friction, the peak deviatoric stress increases, the dilatancy state comes more rapidly, and the degree of dilatancy is more obvious.
- The influence of inter-particle friction on the coordination number of the strong and weak contact networks varies greatly. In the peak deviatoric stress state, the coordination number distribution of the weak contact network is similar to that of the total contact network and greatly affected by μ, while the number of particles forming

the force chain in the strong contact network does not fluctuate. The average coordination number of Γ_{weak} is larger than that of Γ_{strong}, with different inter-particle friction. It can be deduced that the weak contact network contributes greatly to the deformation of granular materials.

- The inter-particle friction has a significant effect on the micro-mechanical properties of the granular assembly, enhancing the contact force between particles and the overall stability. The increase in inter-particle friction results in the decrease of the relative slip behavior between particles, the increasing difference of contact forces between strong and weak contact networks, and the enchanced anisotropy feature of the total network. These phenomena stimulate the strong contact network to strengthen the shear strength to balance the external loads and enhance the ability of the granular assembly to bear macro-stress anisotropy.

REFERENCES

[1] K. Been, M. Jefferies. *Soil Liquefaction: A Critical State Approach.* Taylor & Francis, New York, (2006).

[2] Zhao J, Guo N. A new definition on critical state of granular media accounting for fabric anisotropy[C]// AIP Conference Proceedings. American Institute of Physics, (2013).

[3] Wei Z, Lifu Y, Gang M, et al. Macro-micro responses of crushable granular material in simulated true triaxial test. *Granular Matter* (2015) **17(4)**:497-509.

[4] L. Rothenburg, R. J. Bathurst. Analytical study of induced anisotropy in idealized granular materials. *Géotechnique* (1989), **39**:601-614.

[5] Wei Z, Jiaying L, Gang M, et al. Macroscopic and microscopic behaviors of granular materials under proportional strain path: a DEM study. *International Journal for Numerical and Analytical Methods in Geomechanics* (2016) **40(18)**:2450-2467.

[6] F. Radjai, D. E. Wolf, M. Jean, et al. Bimodal Character of Stress Transmission in Granular Packings. *Physical Review Letters* (1998) **80(1)**:61-64.

[7] F. Radjai, M. Jean, J. J. Moreau, et al.Force Distributions in Dense Two-Dimensional Granular Systems. *Physical Review Letters* (1996) **77(2)**:274-277.

[8] K. Hanley, X. Huang, C. O'Sullivan, et al. Temporal variation of contact networks in granular materials. *Granular Matter* (2014) 16(1):41-54.

[9] Jiaying L, Gang M, Wei. Z et al. Three-dimensional critical state and dilatancy of granular materials based on DEM. Journal of Hydraulic Engineering, (2017) **48(9)**:1107-1117.

[10] Wei Z, Wei W, Gang M, et al. Study of the effects of anistropic consolidation on granular materials under complex stress paths using the DEM. *Granular Matter* (2017) **19(4)**:76.

[11] Zhao J, Guo N. Rotational resistance and shear-induced anisotropy in granular media. *Acta Mechanica Solida Sinica* (2014) **27(1)**:1-14.

[12] Jiaying L, Gang M, Wei Z et al. Contact fabric characteristics of granular materials under three dimensional stress paths. *Chinese Journal of Theoretical and Applied Mechanics* (2019) **51(1)**:34-43.

[13] L. Rothenburg, N. P. Kruyt. Critical state and evolution of coordination number in simulated granular materials. *International Journal of Solids and Structures* (2004) **41(21)**:5763-5774.

[14] Huang X, K. J. Hanley, C. O'Sullivan, et al. Exploring the influence of interparticle friction on critical state behaviour using DEM. *International Journal for Numerical and Analytical Methods in Geomechanics* (2014) **38(12)**.
[15] M. Muthuswamy, A. Tordesillas. How do interparticle contact friction, packing density and degree of polydispersity affect force propagation in particulate assemblies?. *Journal of Statistical Mechanics: Theory and Experiment*, (2006), **2006(09)**:P09003-P09003.
[16] Antony S J, Kruyt N P. Role of interparticle friction and particle-scale elasticity in the shear-strength mechanism of three-dimensional granular media. *Physical Review E* (2009) **79(3)**:031308.
[17] V. Richefeu, M. S. E. Youssoufi, E. Azéma, et al. Force transmission in dry and wet granular media. Powder Technology (2009), 190(1):258-263.
[18] Xing H, K. J. Hanley, C. O'Sullivan, et al. Exploring the influence of interparticle friction on critical state behaviour using DEM. *International Journal for Numerical and Analytical Methods in Geomechanics* (2014) **38(12)**: 1276-1297.
[19] I. Bratberg, F. Radjai, A. Hansen. Dynamic rearrangements and packing regimes in randomly deposited two-dimensional granular beds. *Physical Review E* (2002) **66(3)**:031303.
[20] Jiaying L, Wei Z, Gang M, et al. Strong contacts, connectivity and fabric anisotropy in granular materials: a 3D perspective. *Powder Technology*. Submitted.
[21] S. Yimsiri, K. Soga. DEM analysis of soil fabric effects on behaviour of sand. *G´eotechnique* (2010) **60(6)**:483-495.
[22] M. Satake. The role of the characteristic line in static soil behavior. *IUTAM symposium on Deformation and Failure of Granular Materials* (1982): 63-68.
[23] M. Oda. Fabric tensor for discontinuous geological materials. *Soils and Foundations* (1982) **22(4)**: 96-108.